https://doi.org/10.15407/ujpe66.5.412

A.S. VDOVYCH

Institute for Condensed Matter Physics, Nat. Acad. of Sci. of Ukraine
(1, Svientsitskii Str., Lviv 79011, Ukraine; e-mail: vas@icmp.lviv.ua)

LONGITUDINAL AND TRANSVERSE ELECTROCALORIC EFFECTS IN GLYCINIUM PHOSPHITE FERROELECTRIC

A modified proton ordering model of glycinium phosphite ferroelectric, which involves the piezoelectric coupling of the proton and lattice subsystems, is used for the investigation of the electrocaloric effect. The model also accounts for the dependence of the effective dipole moment on a hydrogen bond on an order parameter, as well as a splitting of parameters of the interaction between pseudospins in the presence of shear stresses. In the two-particle cluster approximation, the influence of longitudinal and transverse electric fields on components of the polarization vector and the dielectric permittivity tensor, as well as on thermal characteristics of the crystal, is calculated. Longitudinal and transverse electrocaloric effects are studied. The calculated electrocaloric temperature change is quite small, about 1K; however, it can change its sign under the influence of a transverse field.

K e y w o r d s: ferroelectrics, phase transition, dielectric permittivity, electric field effect, electrocaloric effect.

1. Introduction

As is known, $NH_3CH_2COOH{\cdot}H_2PO_3$ crystal (glycinium phosphite – GPI) belongs to the family of ferroelectrics with hydrogen bonds [1, 2]. At room temperature, this crystal is in the paraelectric phase and has a monoclinic structure (space group $P2_1/a$) [3–5]. But, at the temperature about 225 K, the crystal passes to the ferroelectric phase (space group $P2_1$). At that, there appear simultaneously ferroelectric ordering of dipole moments along the crystallographic b axis and the antiferroelectric ordering in the (b,c) plane. As a result, the crystal is sensitive to the influence of both: longitudinal and transverse electric fields. In particular, in [6, 7] it was experimentally discovered that its transverse permittivity ε_{zz} in the ferroelectric phase greatly increases under the influence of a transverse field E_z. In addition, dielectric properties of the crystal greatly depend on hydrostatic [8] and uniaxial [9] pressures. These peculiarities make GPI crystals of interest for studies.

In [6, 10], a pseudospin proton ordering model was proposed for the theoretical study of dielectric properties of GPI crystals, which takes the orientation of dipole moments in an unit cell into account. Based on this model, the transverse field effect on the permittivity ε_{zz} was qualitatively properly explained.

In [11], this model was developed by considering the lattice strains and piezoelectric coupling of the proton and lattice subsystems (deformed proton ordering model). This made it possible to calculate expressions for the spontaneous polarization, static dielectric permittivity tensor, piezoelectric coefficients, elastic constants, and molar heat capacity of the crystal and to obtain the good explanation of experimental data for these characteristics. In addition, based on a modified GPI model, the effects of transverse fields E_x and E_z [12] of hydrostatic [13] and uniaxial [14] pressures on the phase transition and thermodynamic characteristics of GPI crystals, as well as

relexational phenomena [15], were quantitatively explained.

Experimental data [16] show that, in the presence of longitudinal field E_y, the phase transition smears, and the temperature dependence of the longitudinal permittivity $\varepsilon_{yy}(T)$ has rounded maximum. At the same time, in the model proposed in [11], the effective dipole moments with different values of longitudinal components in the para- and ferroelectric phases are used for the description of $\varepsilon_{yy}(T)$. This leads to the appearance of a break on the curve $\varepsilon_{yy}(T)$ instead of a smoothed maximum in the presence of the field E_y. Therefore, in [17] for a proper description of the phase transition smearing, the model [11] was modified. It was supposed that the effective dipole moment on a hydrogen bond depends on the order parameter on this bond, because this parameter continuously depends on the temperature near the phase transition point. This made it possible to quantitatively describe the effect of the field E_y.

In [18], the model of GPI proposed in [11] was modified with regard for the splitting of parameters of the interaction between pseudospins under shear stresses ε_4 and ε_6. This enabled the study of the effects of shear stresses σ_4 and σ_6 on the phase transition and on dielectric and piezoelectric characteristics of the crystal.

It is interesting to investigate also the electrocaloric (EC) effect, which is a change the temperature ΔT of the crystal at an adiabatic change of the applied electric field E_y or E_z, on the basis of the deformed proton ordering model. In the present paper, we will simultaneously consider the dependence of the effective dipole moment on a hydrogen bond on the order parameter on this bond, as well as a splitting of parameters of the interaction between pseudospins under shear stresses.

2. The Model of GPI Crystal

The proton ordering model of GPI [11, 18] can be understood from Fig. 1, where a unit cell in the ferroelectric phase is presented. For a better understanding of the model, the only phosphite groups are shown in the figure. Protons, which are localized on O–H ... O bonds between the phosphite groups HPO_3, form zigzag chains along the crystallographic c-axis of the crystal. Dipole moments $\mathbf{d}_{qf}(f = 1, ..., 4)$ are ascribed to the protons on the bonds. In the ferroelectric phase, the dipole moments compensate one another ($\mathbf{d}_{q1}$ with $\mathbf{d}_{q3}$, $\mathbf{d}_{q2}$ with $\mathbf{d}_{q4}$) in the directions Z and X ($X \perp (b, c)$, $Y \parallel b$, $Z \parallel c$), and simultaneously supplement one another in the direction Y, creating the spontaneous polarization.

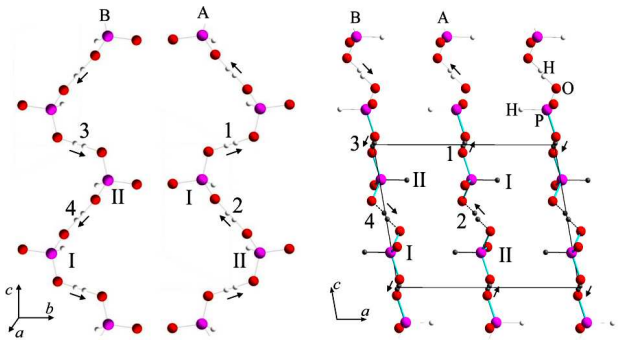

Fig. 1. Orientations of vectors $\mathbf{d}_{qf}$ in a primitive cell in the ferroelectric phase [11, 18]

The pseudospin variables $\frac{\sigma_{q1}}{2}, ..., \frac{\sigma_{q4}}{2}$ describe a reorientation of the dipole moments of the base units: $\mathbf{d}_{qf} = \boldsymbol{\mu}_f \frac{\sigma_{qf}}{2}$. The mean values $\langle \frac{\sigma}{2} \rangle = \frac{1}{2}(n_a - n_b)$ are connected with differences in the occupancies of the two possible molecular positions, n_a and n_b.

Hereinafter for convenience, we use the notations 1, 2, and 3 instead of x, y, and z, respectively, for components of vectors and tensors. The Hamiltonian of the proton subsystem of GPI, which involves the short-range and long-range interactions and the applied mechanical stresses and electric fields E_1, E_2, E_3 along positive directions of the Cartesian axes X, Y, and Z, can be written in such a way:

$$\hat{H} = NU_{\text{seed}} + \hat{H}_{\text{short}} + \hat{H}_{\text{long}} + \hat{H}_E + \hat{H}'_E, \qquad (2.1)$$

where N is the total number of primitive cells. The term U_{seed} in (2.1) is the "seed" energy, which relates to the heavy ion sublattice and does not explicitly depend on the configuration of the proton subsystem. It includes the elastic, piezoelectric, and dielectric parts expressed in terms of electric fields E_i ($i = 1, 2, 3$) and strains ε_j ($j = 1, ..., 6$):

$$U_{\text{seed}} = v\left(\frac{1}{2}\sum_{j,j'=1}^{6} c_{jj'}^{E0}(T)\varepsilon_j\varepsilon_{j'} - \right.$$
$$\left. - \sum_{i=1}^{3}\sum_{j=1}^{6} e_{ij}^{0}\varepsilon_j E_i - \sum_{i,i'=1}^{3}\frac{1}{2}\chi_{ii'}^{\varepsilon 0}E_iE_{i'}\right). \qquad (2.2)$$

The parameters $c_{jj'}^{E0}(T)$, e_{ij}^{0}, $\chi_{ii'}^{\varepsilon 0}$ are so called "seed" elastic constants, "seed" coefficients of piezoelectric

stresses, and "seed" dielectric susceptibilities, respectively; v is the volume of a primitive cell. Matrices $c^{E0}_{jj'}$, e^0_{ij}, $\chi^{\varepsilon 0}_{ii'}$ are given by:

$$\hat{c}^{E0}_{jj'} = \begin{pmatrix} c^{E0}_{11} & c^{E0}_{12} & c^{E0}_{13} & 0 & c^{E0}_{15} & 0 \\ c^{E0}_{12} & c^{E0}_{22} & c^{E0}_{23} & 0 & c^{E0}_{25} & 0 \\ c^{E0}_{13} & c^{E0}_{23} & c^{E0}_{12} & 0 & c^{E0}_{35} & 0 \\ 0 & 0 & 0 & c^{E0}_{44} & 0 & c^{E0}_{46} \\ c^{E0}_{15} & c^{E0}_{25} & c^{E0}_{35} & 0 & c^{E0}_{55} & 0 \\ 0 & 0 & 0 & c^{E0}_{46} & 0 & c^{E0}_{66} \end{pmatrix},$$

$$\hat{e}^0_{ij} = \begin{pmatrix} 0 & 0 & 0 & e^0_{14} & 0 & e^0_{16} \\ e^0_{21} & e^0_{22} & e^0_{23} & 0 & e^0_{25} & 0 \\ 0 & 0 & 0 & e^0_{34} & 0 & e^0_{36} \end{pmatrix}, \tag{2.3}$$

$$\hat{\chi}^{\varepsilon 0}_{ii'} = \begin{pmatrix} \chi^{\varepsilon 0}_{11} & 0 & \chi^{\varepsilon 0}_{13} \\ 0 & \chi^{\varepsilon 0}_{22} & 0 \\ \chi^{\varepsilon 0}_{13} & 0 & \chi^{\varepsilon 0}_{33} \end{pmatrix}.$$

In the paraelectric phase, all coefficients $e^0_{ij} \equiv 0$.

Another terms in (2.1) describe the pseudospin part of the Hamiltonian. In particular, the second term in (2.1) is the Hamiltonian of short-range interactions:

$$\hat{H}_{\text{short}} = -\sum_{qq'} \left(w_1 \frac{\sigma_{q1}}{2} \frac{\sigma_{q2}}{2} + w_2 \frac{\sigma_{q3}}{2} \frac{\sigma_{q4}}{2} \right) \times \\ \times \left(\delta_{\mathbf{R}_q \mathbf{R}_{q'}} + \delta_{\mathbf{R}_q + \mathbf{R_c}, \mathbf{R}_{q'}} \right). \tag{2.4}$$

In (2.4), σ_{qf} is the z-component of the pseudospin operator that describes a state of the f-th bond ($f = 1, 2, 3, 4$) in the q-th cell. The first Kronecker delta corresponds to the interaction between protons in the chains near the tetrahedra HPO_3 of type "I" (see Fig. 1), whereas the second one – near the tetrahedra HPO_3 of type "II", $\mathbf{R_c}$ is the lattice vector along the c-axis. Contributions to the energy of interaction between protons near tetrahedra of different types, as well as the mean values of the pseudospins $\eta_f = \langle \sigma_{qf} \rangle$, which are related to tetrahedra of different types, are identical.

Parameters w_1, w_2, which describe the short-range interactions within the chains, are expanded linearly in the series in strains ε_j:

$$w_1 = w^0 + \sum_j \delta_{1l} \varepsilon_j = w^0 + \sum_l \delta_l \varepsilon_l + \delta_4 \varepsilon_4 + \delta_6 \varepsilon_6, \\ w_2 = w^0 + \sum_j \delta_{2l} \varepsilon_j = w^0 + \sum_l \delta_l \varepsilon_l - \delta_4 \varepsilon_4 - \delta_6 \varepsilon_6, \tag{2.5}$$

where $l = 1, 2, 3, 5$. The third term in (2.1) describes the long-range dipole-dipole interactions and indirect (through the lattice vibrations) interactions between protons, which are taken into account in mean field approximation:

$$\hat{H}_{\text{long}} = \frac{1}{2} \sum_{\substack{qq' \\ ff'}} J_{ff'}(qq') \frac{\langle \sigma_{qf} \rangle}{2} \frac{\langle \sigma_{q'f'} \rangle}{2} - \\ - \sum_{\substack{qq' \\ ff'}} J_{ff'}(qq') \frac{\langle \sigma_{q'f'} \rangle}{2} \frac{\sigma_{qf}}{2}. \tag{2.6}$$

The Fourier transforms of the interaction constants $J_{ff'} = \sum_{q'} J_{ff'}(qq')$ at $\mathbf{k} = 0$ are linearly expanded with respect to the strains ε_j:

$$J_{ff'} = J^0_{ff'} + \sum_j \psi_{ff'j} \varepsilon_l.$$

In view of the symmetry of the crystal, the parameters $J_{ff'}$ are given by:

$$J_{\frac{11}{33}} = J^0_{11} + \sum_l \psi_{11l} \varepsilon_l \pm \psi_{114} \varepsilon_4 \pm \psi_{116} \varepsilon_6, \\ J_{13} = J^0_{13} + \sum_l \psi_{13l} \varepsilon_l + \psi_{134} \varepsilon_4 + \psi_{136} \varepsilon_6, \\ J_{\frac{12}{34}} = J^0_{12} + \sum_l \psi_{12l} \varepsilon_l \pm \psi_{124} \varepsilon_4 \pm \psi_{126} \varepsilon_6, \\ J_{\frac{14}{23}} = J^0_{14} + \sum_l \psi_{14l} \varepsilon_l \pm \psi_{144} \varepsilon_4 \pm \psi_{146} \varepsilon_6, \\ J_{\frac{22}{44}} = J^0_{22} + \sum_l \psi_{22l} \varepsilon_l \pm \psi_{224} \varepsilon_4 \pm \psi_{226} \varepsilon_6, \\ J_{24} = J^0_{24} + \sum_l \psi_{24l} \varepsilon_l + \psi_{244} \varepsilon_4 + \psi_{246} \varepsilon_6, \tag{2.7}$$

As one can see from (2.5), (2.7), the parameters w and most of $J_{ff'}$ split in the presence of shear strains ε_4, ε_6.

As a result, (2.6) can be written as:

$$\hat{H}_{\text{long}} = NH^0 - \sum_q \sum_{f=1}^{4} \mathcal{H}_f \frac{\sigma_{qf}}{2}, \tag{2.8}$$

where

$$H^0 = \sum_{f,f'=1}^{4} \frac{1}{8} J_{ff'} \eta_f \eta_{f'}, \ \mathcal{H}_f = \sum_{f'=1}^{4} \frac{1}{2} J_{ff'} \eta_{f'}. \tag{2.9}$$

The fourth term in (2.1) describes the interactions of pseudospins with the external electric field:

$$\hat{H}_E = -\sum_{qf} \boldsymbol{\mu}_f \, \mathbf{E} \frac{\sigma_{qf}}{2}. \tag{2.10}$$

Here, $\boldsymbol{\mu}_1 = (\mu_{13}^x, \mu_{13}^y, \mu_{13}^z)$, $\boldsymbol{\mu}_3 = (-\mu_{13}^x, \mu_{13}^y, -\mu_{13}^z)$, $\boldsymbol{\mu}_2 = (-\mu_{24}^x, -\mu_{24}^y, \mu_{24}^z)$, $\boldsymbol{\mu}_4 = (\mu_{24}^x, -\mu_{24}^y, -\mu_{24}^z)$ are the effective dipole moments per one pseudospin.

The term $\hat{H}'_E$ in Hamiltonian (2.1) is introduced in the present model for the first time. It accounts for the above-mentioned dependence of the longitudinal components of dipole moments on the mean value of the pseudospin s_f:

$$\hat{H}'_E = -\sum_{qf} s_f^2 \mu'_f E_2 \frac{\sigma_{qf}}{2} = -\sum_{qf} \left(\frac{1}{N} \sum_{q'} \sigma_{q'f} \right)^2 \mu'_f E_2 \frac{\sigma_{qf}}{2}. \tag{2.11}$$

Here corrections to the dipole moments $s_f^2 \mu'_f$ are used instead of $s_f \mu'_f$ because of the symmetry considerations, the energy should not change, when the field and all pseudospins change their sign.

The term $\hat{H}'_E$, as well as long-range interactions, is taken into account in the mean field approximation:

$$\begin{aligned}
\hat{H}'_E &= -\sum_{qf} \left(\frac{1}{N} \sum_{q'} \sigma_{q'f} \right)^2 \mu'_f E_2 \frac{\sigma_{qf}}{2} = \\
&= -\frac{1}{N^2} \sum_{qf} \sum_{q'} \sum_{q''} \sigma_{qf} \sigma_{q'f} \sigma_{q''f} \frac{\mu'_f E_2}{2} \approx \\
&\approx -\frac{1}{N^2} \sum_{qf} \sum_{q'} \sum_{q''} ((\sigma_{qf} + \sigma_{q'f} + \sigma_{q''f}) \eta_f^2 - 2\eta_f^3) \frac{\mu'_f E_2}{2} = \\
&= -\sum_{q} \sum_{f=1}^{4} (3\sigma_{qf} \eta_f^2 - 2\eta_f^3) \frac{\mu'_f E_2}{2} = \\
&= -3 \sum_{q} \sum_{f=1}^{4} \frac{\sigma_{qf}}{2} \eta_f^2 \mu'_f E_2 + N \sum_{f=1}^{4} \eta_f^3 \mu'_f E_2.
\end{aligned} \tag{2.12}$$

The two-particle cluster approximation for short-range interactions is used for the calculation of field effects in GPI. In this approximation, the thermodynamic potential under stresses σ_j is given by:

$$G = NU_{\text{seed}} + NH^0 + N \sum_{f=1}^{4} \eta_f^3 \mu'_f E_2 - Nv \sum_{j=1}^{6} \sigma_j \varepsilon_j - k_{\text{B}} T \sum_{q} \left\{ 2 \ln \operatorname{Sp} e^{-\beta \hat{H}_q^{(2)}} - \sum_{f=1}^{4} \ln \operatorname{Sp} e^{-\beta \hat{H}_{qf}^{(1)}} \right\}, \tag{2.13}$$

where the following notations are used:

$$\operatorname{Sp}\{...\} = \sum_{\sigma_1=\pm 1} \sum_{\sigma_2=\pm 1} \sum_{\sigma_3=\pm 1} \sum_{\sigma_4=\pm 1} \{...\},$$

$\beta = \frac{1}{k_{\text{B}} T}$, k_{B} is the Boltzmann constant, $\hat{H}_q^{(2)}$ and $\hat{H}_{qf}^{(1)}$ are the effective two-particle and one-particle Hamiltonians:

$$\hat{H}_q^{(2)} = H_{sh} - \sum_{f=1}^{4} \frac{y_f}{\beta} \frac{\sigma_{qf}}{2}, \tag{2.14}$$

$$\hat{H}_{qf}^{(1)} = -\frac{\bar{y}_f}{\beta} \frac{\sigma_{qf}}{2}, \tag{2.15}$$

$$H_{sh} = -2 \left(w_1 \frac{\sigma_{q1}}{2} \frac{\sigma_{q2}}{2} + w_2 \frac{\sigma_{q3}}{2} \frac{\sigma_{q4}}{2} \right), \tag{2.16}$$

$$\begin{aligned}
y_f &= \beta(\Delta_1 + \mathcal{H}_f + \boldsymbol{\mu}_f \mathbf{E} + 3\eta_f^2 \mu'_f E_2), \\
\bar{y}_f &= \beta \Delta_f + y_f.
\end{aligned} \tag{2.17}$$

The symbols Δ_f are the effective fields created by the neighboring bonds from outside of the cluster. In the cluster approximation, the fields Δ_f can be determined from the condition of minimum of the thermodynamic potential $\partial G / \partial \Delta_f = 0$, which gives the self-consistency condition that states that the mean values of the pseudospins $\langle \sigma_{qf} \rangle = \eta_f$ calculated with the two-particle and one-particle Gibbs distributions, respectively, should coincide:

$$\eta_f = \frac{\operatorname{Sp} \sigma_{qf} e^{-\beta \hat{H}_q^{(2)}}}{\operatorname{Sp} e^{-\beta \hat{H}_q^{(2)}}} = \frac{\operatorname{Sp} \sigma_{qf} e^{-\beta \hat{H}_{qf}^{(1)}}}{\operatorname{Sp} e^{-\beta \hat{H}_{qf}^{(1)}}}. \tag{2.18}$$

Using (2.18) with the one-particle distribution function ($\eta_f = \operatorname{th}(\bar{y}_f/2)$), the effective fields Δ_f are expressed through the order parameters η_f

$$\Delta_f = \frac{1}{2\beta} \ln \frac{1+\eta_f}{1-\eta_f} - \frac{1}{2} \mathcal{H}_f - \frac{1}{2} (\boldsymbol{\mu}_f \mathbf{E} + 3\eta_f^2 \mu'_f E_2),$$

Then y_f are given by:

$$y_f = \frac{1}{2} \ln \frac{1+\eta_f}{1-\eta_f} + \beta \sum_{f'=1}^{4} \frac{J_{ff'}}{4} \eta_{f'} + \frac{\beta}{2} (\boldsymbol{\mu}_f \mathbf{E} + 3\eta_f^2 \mu'_f E_2).$$

The first equality (2.18) yields the system of equations for the order parameters η_f:

$$\eta_f = \frac{1}{Z} \operatorname{Sp} \left\{ \sigma_{qf} e^{-\beta H_{sh} + \sum_{l=1}^{4} y_l \frac{\sigma_{ql}}{2}} \right\}, \tag{2.19}$$

where Z is the two-particle partition function.

$$Z = \mathrm{Sp}\; e^{-\beta H_{sh} + \sum\limits_{l=1}^{4} y_l \frac{\sigma_{ql}}{2}}. \tag{2.20}$$

3. Thermodynamic Characteristics of GPI

Let us write the thermodynamic potential per unit cell in the form

$$g = \frac{G}{N} = U_{\text{seed}} + H^0 + \sum_{f=1}^{4} \eta_f^3\, \mu'_f\, E_2 - \upsilon \sum_{j=1}^{6} \sigma_j \varepsilon_j + \\ + 4k_{\mathrm{B}}T \ln 2 - \frac{1}{2} k_{\mathrm{B}}T \sum_{f=1}^{4} \ln\bigl(1-\eta_f^2\bigr) - 2k_{\mathrm{B}}T \ln Z. \tag{3.1}$$

From the condition of minimum of the thermodynamic potential, we have

$$\left(\frac{\partial g}{\partial \varepsilon_j}\right)_{E_i,\sigma_j} = 0.$$

Taking (2.19) into account, we get a system of equations for the strains ε_j:

$$\sigma_j = \sum_{j'=1}^{6} c_{jj'}^{E0}(T)\varepsilon_{j'} - \sum_{i=1}^{3} e_{ij}^0\, E_i - \\ - \frac{2M_l}{\upsilon Z} - \sum_{f,f'=1}^{4} \frac{\psi_{ff'l}}{8v}\, \eta_f\, \eta_{f'}. \tag{3.2}$$

Here, the following notation is used:

$$M_l = \mathrm{Sp}\left\{2\left(\delta_{1l}\frac{\sigma_{q1}}{2}\frac{\sigma_{q2}}{2} + \delta_{2l}\frac{\sigma_{q3}}{2}\frac{\sigma_{q4}}{2}\right) e^{-\beta H_{sh} + \sum\limits_{f=1}^{4} y_f \frac{\sigma_{qf}}{2}}\right\}.$$

Differentiating the thermodynamic potential with respect to the fields E_i, one can get the expressions for components of the polarization P_i:

$$\begin{aligned} P_1 &= e_{14}^0\varepsilon_4 + e_{16}^0\varepsilon_6 + \chi_{11}^{\varepsilon 0}E_1 + \\ &+ \frac{1}{2v}[\mu_{13}^x(\eta_1-\eta_3) - \mu_{24}^x(\eta_2-\eta_4)], \\ P_2 &= e_{21}^0\varepsilon_1 + e_{22}^0\varepsilon_2 + e_{23}^0\varepsilon_3 + e_{25}^0\varepsilon_5 + \chi_{22}^{\varepsilon 0}E_2 + \\ &+ \frac{1}{2v}[\mu_{13}^y(\eta_1+\eta_3) - \mu_{24}^y(\eta_2+\eta_4)] + \frac{1}{2v}\sum_{f=1}^{4}\eta_f^3\mu'_f, \\ P_3 &= e_{34}^0\varepsilon_4 + e_{66}^0\varepsilon_6 + \chi_{33}^{\varepsilon 0}E_3 + \\ &+ \frac{1}{2v}[\mu_{13}^z(\eta_1-\eta_3) + \mu_{24}^z(\eta_2-\eta_4)]. \end{aligned} \tag{3.3}$$

The components of the isothermic dielectric susceptibility tensor of mechanically clamped or free crystal GPI can be found by the numerical differentiation of components of the polarization vector with respect to components of the field at a constant strain or constant stress, respectively:

$$\chi_{ii'}^{\varepsilon} = \lim_{E_{i'}\to 0}\left(\frac{\partial P_i}{\partial E_{i'}}\right)_{\varepsilon_j}, \quad \chi_{ii'}^{\sigma} = \lim_{E_{i'}\to 0}\left(\frac{\partial P_i}{\partial E_{i'}}\right)_{\sigma_j},$$

The molar entropy of the proton subsystem (here, R is the gas constant) is given by:

$$S = -\frac{N_A}{4}\left(\frac{\partial g}{\partial T}\right)_{\eta,\varepsilon_i} = \frac{R}{4}\left\{-4\ln 2 + \frac{1}{2}\sum_{f=1}^{4}\ln(1-\eta_f) + \\ + 2\ln Z - \frac{2\beta}{Z}\mathrm{Sp}\left\{H_{2\beta}e^{-\beta H_{sh} + \sum\limits_{f=1}^{4} y_f \frac{\sigma_{qf}}{2}}\right\}\right\}, \tag{3.4}$$

where such notation is used:

$$H_{2\beta} = -H_{sh} + \sum_{f=1}^{4}\left(\sum_{f'=1}^{4}\frac{J_{ff'}}{4}\eta_{f'} + \\ + \frac{1}{2}(\boldsymbol{\mu}_f\mathbf{E} + 3\eta_f^2\mu'_f E_2)\right)\frac{\sigma_{qf}}{2}.$$

The molar heat capacity of the proton subsystem of GPI crystals can be found by the numerical differentiation of entropy (3.4):

$$\Delta C^{\sigma} = T\left(\frac{\partial S}{\partial T}\right)_{\sigma}. \tag{3.5}$$

The total specific heat is considered to be the sum of the proton and lattice contributions:

$$C = \Delta C^{\sigma} + C_{\text{lattice}}. \tag{3.6}$$

The lattice contribution near T_c is approximated by the linear dependence

$$C_{\text{lattice}} = C_0 + C_1(T - T_c). \tag{3.7}$$

The corresponding lattice contribution to the entropy near T_c is then

$$S_{\text{lattice}} = \int \frac{C_{\text{lattice}}}{T}dT = (C_0 - C_1T_c)\ln(T) + C_1T. \tag{3.8}$$

Hence, the total entropy as a function of the temperature and the field component E_i reads

$$S_{\text{total}}(T, E_i) = S + S_{\text{lattice}}. \tag{3.9}$$

Solving (3.9) with respect to the temperature at $S_{\rm total}(T, E_i) = \text{const}$ and two values of the field, one can calculate the electrocaloric temperature shift (as seen in Fig. 10)

$$\Delta T = T(S_{\rm total},\, E_i(2)) - T(S_{\rm total},\, E_i(1)). \qquad (3.10)$$

The electrocaloric temperature change can be calculated also, by using the known formula

$$\Delta T = -\int\limits_0^{E_i} \frac{TV}{C}\left(\frac{\partial P_i}{\partial T}\right)_{E_i} dE_i, \qquad (3.11)$$

where $V = vN_A/4$ is the molar volume.

4. Results of Numerical Calculations. Discussion

For the numerical calculation of the dielectric characteristics of GPI, we use the parameters determined in [18] and earlier in [11] from the condition of agreement of the calculated characteristics with experimental data. At that, experimental data on the temperature dependences of the spontaneous polarization $P_s(T)$ [19], molar heat capacity $C_p(T)$ [20], components of the dielectric permittivity $\varepsilon^{\sigma}_{22}$ [21, 22], $\varepsilon^{\sigma}_{11}$, $\varepsilon^{\sigma}_{33}$ [1], piezoelectric coefficients d_{21}, d_{23}[22], as well as the dependences of the phase transition temperature on the hydrostatic pressure $T_c(p)$ [8, 23], were used. The results of lattice dynamics simulations [24] were taken into account as well. The optimal values of the theory parameters are given below.

The parameter of the short-range interactions $w_0/k_{\rm B} = = 800$ K.

The parameters of the long-range interactions:

$\tilde{J}^0_{11} = \tilde{J}^0_{12} = \tilde{J}^0_{22} = 6.23$ K,
$\tilde{J}^0_{13} = \tilde{J}^0_{14} = \tilde{J}^0_{24} = 6.03$ K,

where $\tilde{J}^0_{ff'} = J^0_{ff'}/k_{\rm B}$.

Strain potentials:

$\tilde{\delta}_1 = 500$ K, $\tilde{\delta}_2 = 600$ K, $\tilde{\delta}_3 = 500$ K, $\tilde{\delta}_4 = 150$ K,
$\tilde{\delta}_5 = 100$ K, $\tilde{\delta}_6 = 150$ K; $\tilde{\delta}_i = \delta_i/k_{\rm B}$;
$\tilde{\psi}_{ff'1} = 187.3$ K, $\tilde{\psi}_{ff'2} = 505.1$ K, $\tilde{\psi}_{ff'3} = 221.3$ K,
$\tilde{\psi}_{ff'5} = 45.4$ K,
$\tilde{\psi}_{114} = \tilde{\psi}_{124} = \tilde{\psi}_{224} = \tilde{\psi}_{116} = \tilde{\psi}_{126} = \tilde{\psi}_{226} = 317.8$ K,
$\tilde{\psi}_{134} = \tilde{\psi}_{144} = \tilde{\psi}_{244} = \tilde{\psi}_{136} = \tilde{\psi}_{146} = \tilde{\psi}_{246} = 0.0$ K.

where $\tilde{\psi}_{ff'j} = \psi_{ff'j}/k_{\rm B}$.

Components of the effective dipole moments

$\mu^x_{13} = 0.4\times10^{-18}$ esu·cm; $\mu^y_{13} = 4.05\times10^{-18}$ esu·cm;
$\mu^z_{13} = 4.2\times10^{-18}$ esu·cm; $\mu^x_{24} = 2.3\times10^{-18}$ esu·cm;
$\mu^y_{24} = 3.0\times10^{-18}$ esu·cm; $\mu^z_{24} = 2.2\times10^{-18}$ esu·cm.

Corrections to the effective dipole moments $\mu'_1 = = \mu'_3 = -0.25\times10^{-18}$ esu·cm and $\mu'_2 = \mu'_4 = = 0$ esu·cm are found in the present paper from the condition of agreement of the calculated saturation polarization with experimental data.

The volume of a unit cell of GPI is $\upsilon = 0.601\times \times 10^{-21}$ cm^3.

The "seed" coefficients of the piezoelectric stress e^0_{ij}, "seed" dielectric susceptibilities $\chi^{\varepsilon 0}_{ij}$, and "seed" elastic constants c^{E0}_{ij} are obtained as follow: $e^0_{ij} = 0.0$ $\frac{\rm esu}{\rm cm^2}$; $\chi^{\varepsilon 0}_{11} = 0.1$, $\chi^{\varepsilon 0}_{22} = 0.403$, $\chi^{\varepsilon 0}_{33} = 0.5$, $\chi^{\varepsilon 0}_{31} = 0.0$; $c^{0E}_{11} = 269.1$ kbar, $c^{E0}_{12} = 145$ kbar, $c^{E0}_{13} = 116.4$ kbar, $c^{E0}_{15} = 39.1$ kbar, $c^{E0}_{22} = (649.9 - 0.4(T - T_c))$ kbar, $c^{E0}_{23} = 203.8$ kbar, $c^{E0}_{25} = 56.4$ kbar, $c^{E0}_{33} = 244.1$ kbar, $c^{E0}_{35} = -28.4$ kbar, $c^{E0}_{55} = 85.4$ kbar, $c^{E0}_{44} = 153.1$ kbar, $c^{E0}_{46} = -11$ kbar, $c^{E0}_{66} = 118.8$ kbar.

The parameters of lattice contribution to the molar heat capacity (see (3.7)): $C_0 = 147.5$ J/(mol·K), $C_1 = 0.45$ J/(mol·K^2).

Let us investigate firstly, how the present theory describes the dielectric properties of GPI. In the absence of a field, the spontaneous polarization P_2 monotonically and continuously decreases with increasing the temperature and goes to zero at the temperature T_c (Fig. 2, curve *0*). For comparison, we also present the temperature dependences calculated in [17] $P_2(T)$ (curve *0′*) with regard for the dependence of the effective dipole moment $\mu(\eta)$ on the order parameter, but omitting the splittings of the parameters w and $J_{ff'}$ in the presence of shear strains. Besides, we present the temperature dependences calculated in [18] $P_2(T)$ (curve *0″*) in view of the splittings of the parameters w and $J_{ff'}$, but not accounting for $\mu(\eta)$.

The longitudinal electric field E_2 smears the phase transition. As a result, the curve $P_2(T)$ become smoothed (Fig. 2, curves 2^y, 4^y). In this and next figures in the notations of the curves "a^y, a^z," number a means a value of an external field in MV/m, indices y and z mean the directions of the field (E_y, E_z).

The transverse field E_3 induces the polarization component P_3 (Fig. 3) and lowers the temperature T_c, as it is shown in Fig. 4. In a weak transverse field, the phase transition remains the second order one. At

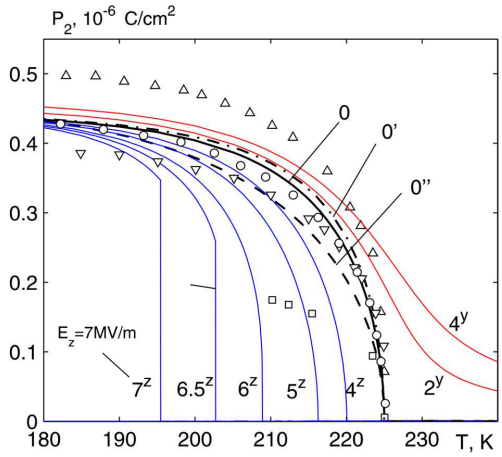

Fig. 2. Temperature dependences of the longitudinal polarization P_2 of GPI crystal at different values of the electric fields E_2 and E_3. Curves 0 (the present result), 0'[17], 0"[18], as well as symbols ○ [19], △ [1], □ [22], ▽ [16] correspond to zero field

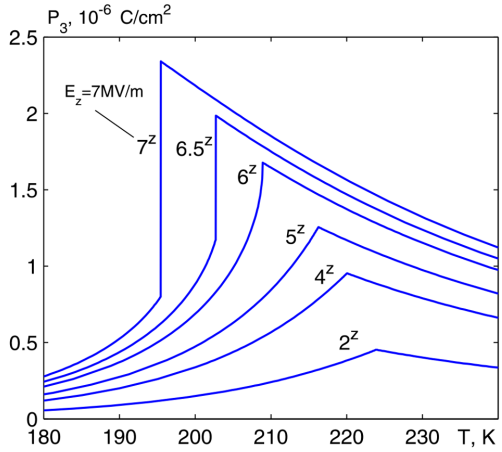

Fig. 3. Temperature dependences of the transverse polarization P_3 of GPI crystal at different values of the field E_3

that, the temperature dependence $P_2(T)$ is qualitatively similar to the case of $E_3 = 0$ MV/m (Fig. 2, curves *4*^{z}, *5*^{z}), the curve $P_3(T)$ has a sharp bend at T_c (Fig. 3, curves *2*^{z}, *4*^{z}, *5*^{z}). In the fields stronger than some critical $E^{\rm tr} \approx 5.9$ MV/m (tricritical point), the phase transition becomes the first order one (dashed curve in Fig. 4). As a result, the components $P_2(T)$ and $P_3(T)$ have a break at T_c (curves *6*^{z}, *6.5*^{z}, *7*^{z} in Fig. 2 and 3).

In the absence of a field, the longitudinal dielectric permittivities of mechanically free $\varepsilon_{22}^{\sigma}$ and clamped $\varepsilon_{22}^{\varepsilon}$ crystals go to infinity at T_c (Fig. 5, solid 1 and dashed *1*′ curves, respectively; as well as Fig. 6,

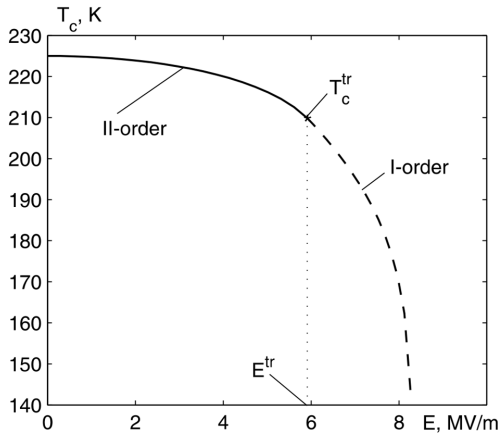

Fig. 4. Dependence of the transition temperature T_c of GPI crystal on the transverse field E_3

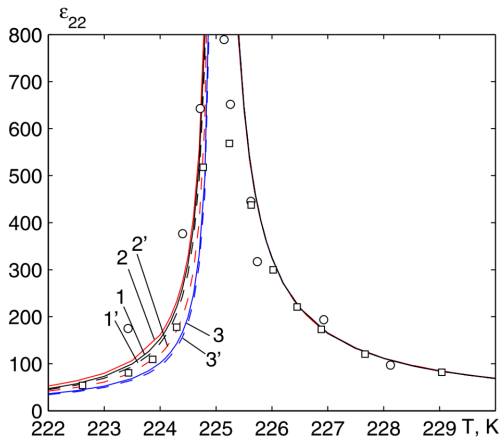

Fig. 5. Temperature dependences of the longitudinal dielectric permittivities of mechanically free $\varepsilon_{22}^{\sigma}$ (solid lines) and clamped $\varepsilon_{22}^{\varepsilon}$ (dashed lines) GPI crystals in the absence of a field; symbols are experimental data of [21] (○), [22] (□). Curves *1*, *1*′ are calculated in the present paper; *2*, *2*′ – in [17]; *3*, *3*′ – in [18]

curves *0*, solid and dashed, respectively). In the paraelectric phase, the permittivities $\varepsilon_{22}^{\sigma}$ and $\varepsilon_{22}^{\varepsilon}$ coincide. For comparison, we also present the temperature dependences $\varepsilon_{22}^{\sigma,\varepsilon}(T)$ calculated in [17] (Fig. 5, curves *2*, *2*′) with regard for $\mu(\eta)$, but omitting the splittings of the parameters w and $J_{ff'}$ in the presence of shear strains. In addition, we give the temperature dependences calculated in [18] $\varepsilon_{22}^{\sigma,\varepsilon}(T)$ (Fig. 5, curves *3*, *3*′), by considering the splittings of the parameters w and $J_{ff'}$, but not accounting for $\mu(\eta)$.

In the presence of a longitudinal electric field E_2, the curves $\varepsilon_{22}^{\sigma,\varepsilon}(T)$ are smoothed (Fig. 6, curves *1*^{y},

2^y, 4^y, as well as Fig. 7). In Fig. 7, black lines are the present results, and red lines are calculated in [17] without regard for the splittings of the parameters w and $J_{ff'}$. It is necessary to note that the curves $\varepsilon_{22}^{\sigma}(T)$, which are calculated for the fields $E_2 = 20$, 30, 40, 70, 120, 170, and 220 kV/m, quite well agree with the experimental data [16], which were measured at the fields $E_2 = 0$, 10, 20, 50, 100, 150, and 200 kV/m. This points to the presence of some internal longitudinal electric field $E_{2in} = 20$ kV/m in the crystal [16]. The experimental data [16] for $\varepsilon_{22}^{\sigma}(T)$ in the absence of a field are one and a half times overstated in comparison with experimental data of another papers. Therefore, for the theoretical description of data [16], we suppose that, in this sample, the parameters $\mu_{13}^{y} = 4.32 \times 10^{-18}$ esu $\cdot$ cm, but all other parameters are such as obtained in [18].

In a weak transverse field $E_3 < E^{\rm tr}$, the longitudinal dielectric permittivity of a mechanically free crystal $\varepsilon_{22}^{\sigma}$ goes to infinity at T_c (Fig. 6, solid lines 4^z, 5^z), whereas the permittivity of a clamped crystal $\varepsilon_{22}^{\varepsilon}$ is finite (Fig. 6, dashed lines 4^z, 5^z). Curves $\varepsilon_{22}^{\sigma}(T)$ and $\varepsilon_{22}^{\varepsilon}(T)$ do not coincide even in the paraelectric phase. In a strong field $E_3 > E^{\rm tr}$, owing to the first-order phase transition, the permittivities $\varepsilon_{22}^{\sigma,\varepsilon}$ both become finite and decrease with increasing the field strength (Fig. 6, curves 6^z, 6.5^z, 7^z).

In the absence of a field, the transverse dielectric permittivities of mechanically free $\varepsilon_{22}^{\sigma}$ and clamped $\varepsilon_{33}^{\varepsilon}$ crystals are finite and have sharp bends at T_c (Fig. 8, solid line 0 and, very close to it, dashed line 0, respectively). In the paraelectric phase, the permittivities $\varepsilon_{33}^{\sigma}$ and $\varepsilon_{33}^{\varepsilon}$ coincide. For comparison, we present the temperature dependences $\varepsilon_{33}^{\sigma}(T)$ [17] (Fig. 8, curve $0'$) with taking $\mu(\eta)$ into account, but not considering the splittings of the parameters w and $J_{ff'}$ in the presence of shear strains.

In the presence of a longitudinal field, the curves $\varepsilon_{33}^{\sigma}(T)$ and $\varepsilon_{33}^{\varepsilon}$ also become smoothed (Fig. 8, solid and dashed curves 4^y). In the presence of a transverse field, the transverse dielectric permittivities $\varepsilon_{33}^{\sigma,\varepsilon}$ greatly increase in the ferroelectric phase in comparison with the case of $E_3 = 0$, and curve $\varepsilon_{33}^{\sigma}(T)$ has a break at T_c (Fig. 8, curves 4^z, 5^z). As was shown in [25], such increase of $\varepsilon_{33}^{\sigma,\varepsilon}$ is related to the disordering of pseudospins in the chain "B" (see Fig.1) at the influence of the field E_3. The maximum value of $\varepsilon_{33}^{\sigma,\varepsilon}$ goes to infinity, when $E_3 \to E^{\rm tr}$. In a strong field $E_3 > E^{\rm tr}$ owing to the first-order phase transition,

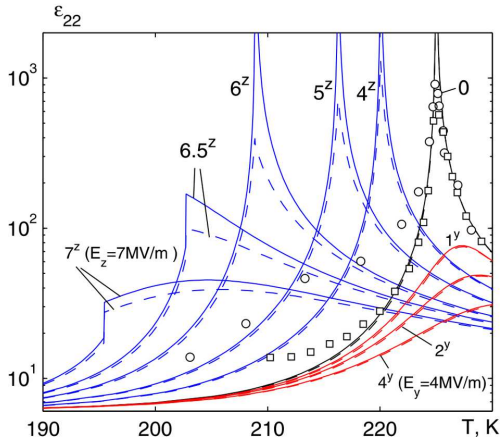

Fig. 6. Temperature dependences of the longitudinal dielectric permittivities of mechanically free $\varepsilon_{22}^{\sigma}$ (solid lines) and clamped $\varepsilon_{22}^{\varepsilon}$ (dashed lines) GPI crystals at different values of the fields E_2 and E_3. Symbols are experimental data [21] (○), [22] (□) without a field

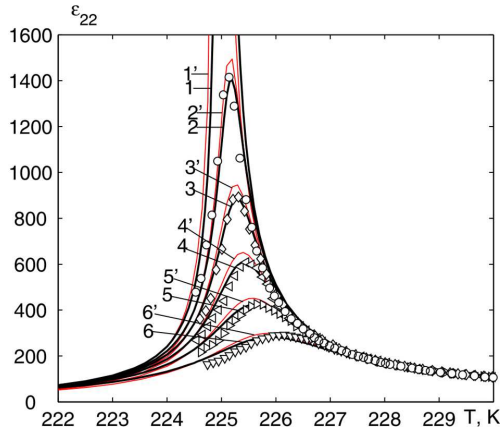

Fig. 7. Temperature dependences of the dielectric permittivity $\varepsilon_{22}^{\sigma}$ of GPI crystal at different values of the field E_2 (MV/m): 0.0 – *1*, *1′*; 0.02 – *2*, *2′* (○); 0.04 – *3*, *3′* (◊); 0.07 – *4*, *4′* (◁); 0.12 – *5*, *5′* (▷); 0.22 – *6*, *6′* (▽). Symbols are experimental data [16]

the permittivities $\varepsilon_{33}^{\sigma,\varepsilon}$ decrease again with increasing the field strength (Fig. 8, curves 6^z, 6.5^z, 7^z, 8^z).

In the presence of the field E_3, experimental curves $\varepsilon_{33}^{\sigma}(T)$ are smoothed near T_c and have no any break (Fig. 9). In order to explain such behavior of the transverse permittivity, we calculated $\varepsilon_{33}^{\sigma}(T)$, by supposing that an internal electric field E_2 appears together with the applied external field E_3. It turned out that it is possible to achieve the satisfactory description of the temperature dependence of $\varepsilon_{33}^{\sigma}$, by supposing that $E_2 \sim 0.07E_3$ (Fig. 9, solid black

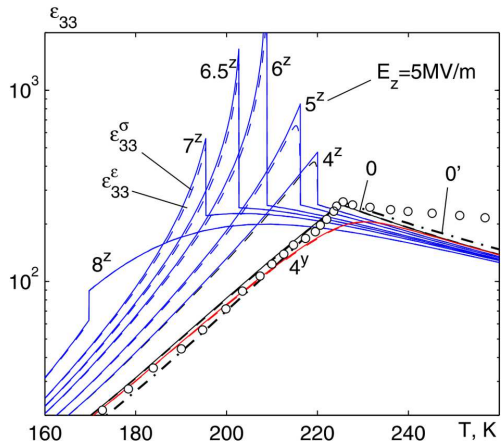

Fig. 8. Temperature dependences of the transverse dielectric permittivities of mechanically free $\varepsilon_{33}^{\sigma}$ (solid lines) and clamped $\varepsilon_{33}^{\varepsilon}$ (dashed lines) GPI crystals at different values of the fields E_2 and E_3; symbols ∘ are experimental data [1] at the zero field

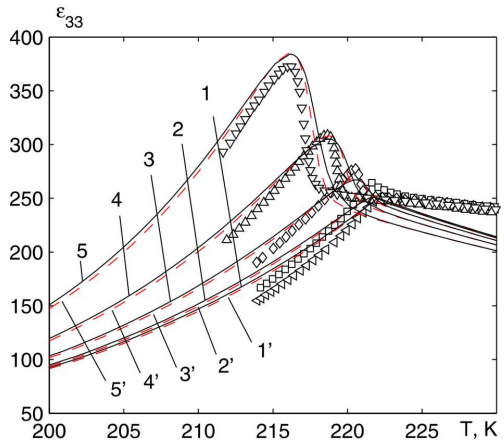

Fig. 9. Temperature dependences of the dielectric permittivity $\varepsilon_{33}^{\sigma}$ at different values of the field strength E_3(MV/m): 0.0 – *1* (◁); 1.0 – *2* (□); 2.0 – *3* (◇); 3.0 – *4* (△); 4.0 – *5* (▽) [7] and at the applied simultaneously longitudinal field $E_2 = 0.07E_3$. Red dashed curves *1′–5′* [25] of the permittivity $\varepsilon_{33}^{\varepsilon}$ at the same values of E_3 and at the field $E_2 \sim 0.05E_3$ applied simultaneously

curves). In this figure, the permittivity calculated in [25] of a mechanically clamped crystal $\varepsilon_{33}^{\varepsilon}$ is shown at different values of the field E_3 and at applied simultaneously longitudinal field $E_2 \sim 0.05E_3$ (dashed red curves). We note that the y-components of the effective dipole moment was considered in [25] to be the same in the paraelectric and ferroelectric phases. It is necessary to note that the phase transition temperature for the sample in [7] was 222 K. For the explanation of the experimental data [7], we supposed that the values of all interactions in this sample are proportional to the values of corresponding interactions in the sample with $T_c = 225$ K: $w^0(222\ \text{K}) = kw^0(225\ \text{K})$, $\nu_f^{0\pm}(222\ \text{K}) = k\nu_f^{0\pm}(225\ \text{K})$, $\delta_i(222\ \text{K}) = k\delta_i(225\ \text{K})$, $\psi_{fi}^{\pm}(222\ \text{K}) = k\psi_{fi}^{\pm}(225\ \text{K})$, $\boldsymbol{\mu}_f(222\ \text{K}) = k\boldsymbol{\mu}_f(225\ \text{K})$, where $k = 0.987 \approx 222/225$. All another parameters are such as for the sample with $T_c = 225$ K.

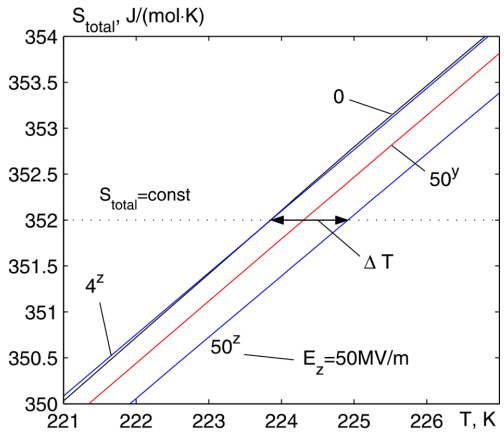

Fig. 10. Temperature dependences of the molar entropy of GPI at different values of the fields E_2 and E_3

The longitudinal field E_2 decreases the entropy of a crystal in the whole temperature interval (Fig. 10, curve 50^y), inasmuch as it increases the ordering of pseudospins in both sublattices, "A" and "B" (Fig. 1). The transverse field E_3 also decreases the entropy, but only in the paraelectric phase. In the ferroelectric phase in the weak fields $E_3 < E^{\text{tr}}$, the entropy increases owing to a disordering of pseudospins in sublattice "B" under the influence of the field E_3 (Fig. 10, curve 4^z). The strong field $E_3 > E^{\text{tr}}$ overturns the pseudospins in sublattice "B" and orders them in its direction. As a result, the entropy decreases again (Fig. 10, curve 50^z).

The effect of the fields E_2 and E_3 on the molar heat capacity is mainly similar to the effect of these fields on the dielectric properties: the field E_2 smoothes the curve $C(T)$ near T_c (Fig. 11, curve 4^y), whereas the field E_3 lowers T_c (Fig. 11, curves 4^z, 5^z, 6^z, 6.5^z, 7^z).

As one can see from the previous figures, the present model, which simultaneously involves $\mu(\eta)$ and the splittings of the interaction parameters w and $J_{ff'}$ in the presence of shear strains, practically reproduces the results of previous calculations [17] and

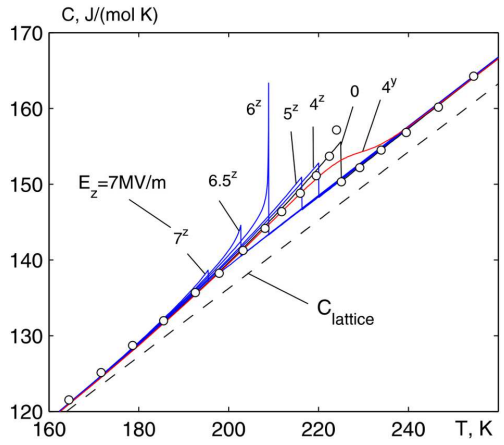

Fig. 11. Temperature dependences of the heat capacity of GPI at different values of the fields E_2 and E_3. Symbols ∘ are experimental data [20]. Solid line presents the result of calculations, the dashed line corresponds to the lattice contribution

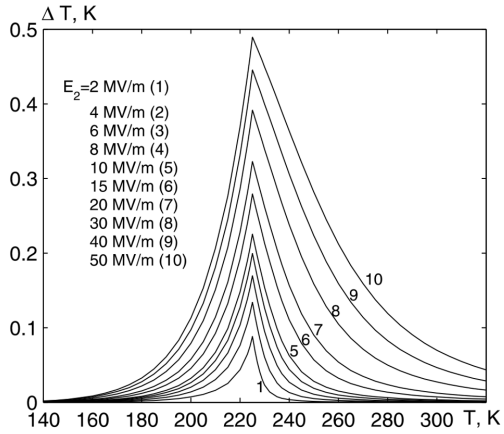

Fig. 12. Temperature dependence of the electrocaloric temperature change ΔT of GPI crystal at different values of the field E_2

[18], as well as satisfactorily describes the experimental data for dielectric characteristics and the effect of electric fields on the dielectric permittivity. Therefore, this model can be suitable for the investigation of the electrocaloroc effect in GPI crystals.

Let us firstly examine the longitudinal EC effect. In Fig. 12, 13, a change of the temperature ΔT of the crystal at the adiabatic change of the applied electric field E_2 at different values of the initial temperature and the field E_2 are presented. In the weak fields ($E_2 < 1\text{MV/m}$) at the initial temperature $T = T_c = 225$ K, the temperature change follows the law $\Delta T \sim E_2^{2/3}$ (green curve in Fig. 13); at

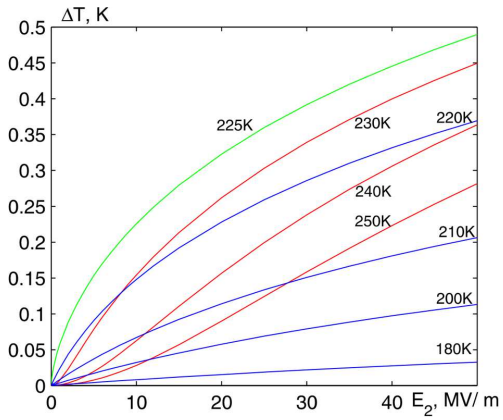

Fig. 13. Dependence of ΔT on the field E_2 at different initial temperatures

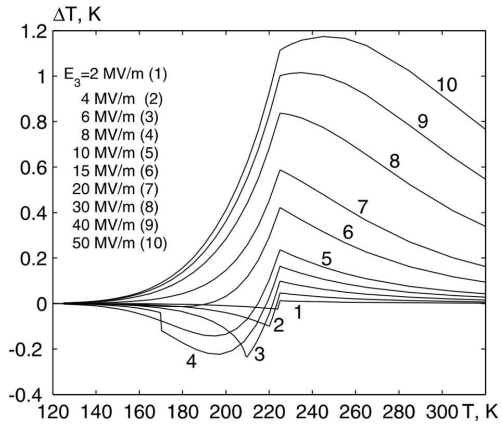

Fig. 14. Temperature dependence of a change in the electrocaloric temperature of GPI crystal at different values of the field E_3

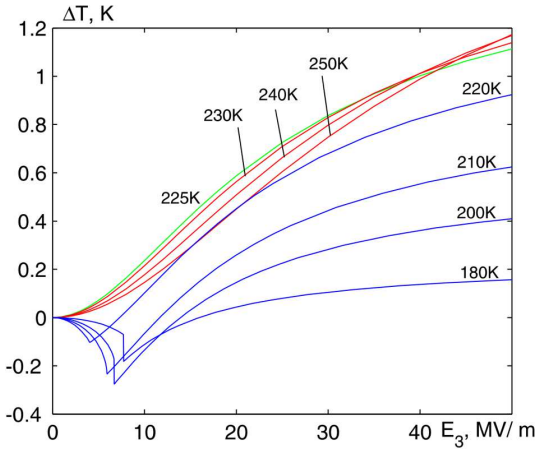

Fig. 15. Dependence of ΔT on the field E_3 at different initial temperatures

$T < T_c$, $\Delta T \sim E_2$ (blue curves in Fig. 13); at $T > T_c$, $\Delta T \sim E_2^2$ (red curves in Fig. 13). At stronger fields $E_2 > 1$MV/m, the dependences $\Delta T(E_2)$ deviate from the mentioned laws and reach the saturation at $E_2 \gg 50$ MV/m. The longitudinal EC effect is positive in the whole temperature interval.

In the case of adiabatic application of a transverse field E_3, the electrocaloric temperature change ΔT can be positive or negative (Fig. 14, 15). At the initial temperatures $T \geqslant T_c$, the transverse EC effect is qualitatively similar to the longitudinal EC effect: in the weak fields $\Delta T \sim E_3^2$ (green and red curves in Fig. 15). At strong fields, the dependences $\Delta T(E_3)$ deviate from the quadratic law and reach the saturation at $E_2 \gg 50$ MV/m. At the initial temperatures $T < T_c$ in the weak fields $E_3 < E^{\rm tr}$, the temperature of the crystal nonlinearly lowers with increasing the field strength (blue curves in Fig. 15). This is connected with the above-mentioned disordering of pseudospins in sublattice "B" under influence of the field E_3 that leads to increasing the entropy at a constant temperature (Fig. 10, curve 4^z) and to the adiabatic (at a constant entropy) lowering of the temperature. In addition, as one can see from Fig. 3, in the ferroelectric phase the the polarization component P_3 increases with the temperature, i.e., $\partial P_3/\partial E_3 > 0$. Then $\Delta T < 0$, according to (3.11). At a further strengthening of the field ($E_3 > E^{\rm tr}$), as was said above, the pseudospins in sublattice "B" turn over and order in the direction of field that leads to decreasing the entropy at a constant temperature (Fig. 10, curve 50^z) and an isoentropic increase of the temperature.

5. Conclusions

The simultaneous consideration of the dependence of the effective dipole moment of a hydrogen bond on the order parameter on this bond $\mu(\eta)$, as well as the splittings of the interaction parameters w and $J_{ff'}$ in the presence of shear strains, practically reproduces the results of previous calculations of the dielectric characteristics with regard for only $\mu(\eta)$ or only the splitting of w and $J_{ff'}$.

At the weak field E_2 in the ferroelectric phase, an electrocaloric temperature change ΔT linearly increases with the field, in the paraelectric phase – quadratically, and at the initial temperature $T = T_c$ – by the law $\Delta T \sim E_2^{2/3}$. At strong fields, the dependence $\Delta T(E_2)$ deviates from these laws and reaches the saturation at $E_2 \gg 50$ MV/m.

The transverse EC effect is qualitatively similar to the longitudinal EC effect, whereas, in the ferroelectric phase, it can be negative. This is connected with the antiferroelectric ordering in the plane (a, c) below T_c.

It should be noted that the present deformed proton ordering model is suitable for studies of the barocaloric, piezocaloric, and multicaloric effects in GPI crystals.

The author is indebted to Prof. R.R. Levitskii and I.R. Zachek for useful remarks.

1. S. Dacko, Z. Czapla, J. Baran, M. Drozd. Ferroelectricity in Gly·H_3PO_3 crystal. *Phys. Lett. A* **223**, 217 (1996).
2. J. Baran, G. Bator, R. Jakubas, M. Sledz. Dielectric dispersion and vibrational studies of a new ferroelectric, glycinium phosphite crystal. *J. Phys.: Condens. Matter* **8**, 10647 (1996).
3. M.-T. Averbuch-Pouchot. Structures of glycinium phosphite and glycylglycinium phosphite. *Acta Crystalogr. C* **49**, 815 (1993).
4. F. Shikanai, M. Komukae, Z. Czapla, T. Osaka. Crystal structure of $NH_3CH_2COOH{\times}H_2PO_3$ in the ferroelectric phase. *J. Phys. Soc. Jpn.* **71**, 498 (2002).
5. H. Taniguchi, M. Machida. N. Koyano. Neutron diffraction study of crystal structures of glycinium phosphite $NH_3CH_2COOH{\times}H_2PO_3$ in paraelectric and ferroelectric phases. *J. Phys. Soc. Jpn.* **72**, 1111 (2003).
6. I. Stasyuk, Z. Czapla, S. Dacko, O. Velychko. Proton ordering model of phase transitions in hydrogen bonded ferrielectric type systems: The GPI crystal. *Condens. Matter Phys.* **6**, 483 (2003).
7. I. Stasyuk, Z. Czapla, S. Dacko, O. Velychko. Dielectric anomalies and phase transition in glycinium phosphite crystal under the influence of a transverse electric field. *J. Phys.: Condens. Matter* **16**, 1963 (2004).
8. N. Yasuda, T. Sakurai, Z. Czapla. Effects of hydrostatic pressure on the paraelectric–ferroelectric phase transition in glycine phosphite (Gly·H_3PO_3). *J. Phys.: Condens Matter* **9**, L347 (1997).
9. T. Kikuta, Y. Takemoto, T. Yamazaki, N. Nakatani. Influence of uniaxial pressure on the phase transition of partially deuterated glycinium phosphite. *Ferroelectrics* **302**, 99 (2004).
10. I. Stasyuk, O. Velychko. Theory of electric field influence on phase transition in glycine phosphite. *Ferroelectrics* **300**, 121 (2004).
11. I.R. Zachek, Ya. Shchur, R.R. Levitskii, A.S. Vdovych. Thermodynamic properties of ferroelectric

$NH_3CH_2COOH \cdot H_2PO_3$ crystal. *Physica B* **520**, 164 (2017).
12. I.R. Zachek, R.R. Levitskii, A.S. Vdovych, I.V. Stasyuk. Influence of electric fields on dielectric properties of GPI ferroelectric. *Condens. Matter Phys.* **20**, 23706 (2017).
13. I.R. Zachek, R.R. Levitskii, A.S. Vdovych. Influence of hydrostatic pressure on thermodynamic characteristics of $NH_3CH_2COOH{\cdot}H_2PO_3$ type ferroelectric materials. *Condens. Matter Phys.* **20**, 43707 (2017).
14. I.R. Zachek, R.R. Levitskii, A.S. Vdovych. The influence of uniaxial pressures on thermodynamic properties of the GPI ferroelectric. *J. Phys. Stud.* **21**, 1704 (2017).
15. I.R. Zachek, R.R. Levitskii, A.S. Vdovych, O.B. Bilenka. Dynamic properties of $NH_3CH_2COOH{\cdot}H_2PO_3$ ferroelectric. *Condens. Matter Phys.* **21**, 13704: 1 (2018).
16. R. Tchukvinskyi, R. Cach, Z. Czapla, S. Dacko. Characterization of ferroelectric phase transition in GPI crystal. *Phys. Stat. Sol. (a)* **165**, 309 (1998).
17. A.S. Vdovych, I.R. Zachek, R.R. Levitskii. Influence of longitudinal electric field on thermodynamic properties of $NH_3CH_2COOH{\cdot}H_2PO_3$ ferroelectric. *Ukr. J. Phys.* **63**, 350 (2018).
18. I.R. Zachek, R.R. Levitskii, A.S. Vdovych. Deformation effects in glycinium phosphite ferroelectric. *Condens. Matter Phys.* **21**, 33702 (2018).
19. J. Nayeem, T. Kikuta, N. Nakatani, F. Matsui, S.-N. Takeda, K. Hattori, H. Daimon. Ferroelectric phase transition character of glycine phosphite. *Ferroelectrics* **332**, 13 (2006).
20. F. Shikanai, J. Hatori, M. Komukae, Z. Czapla, T. Osaka. Heat capacity and thermal expansion of $NH_3CH_2COOH\times$ $\times H_2PO_3$. *J. Phys. Soc. Jpn.* **73**, 1812 (2004).
21. J. Nayeem, H. Wakabayashi, T. Kikuta, T. Yamazaki, N. Nakatani. Ferroelectric properties of deuterated glycine phosphite. *Ferroelectrics* **269**, 153 (2002).
22. M. Wiesner. Piezoelectric properties of GPI crystals. *Phys. Stat. Sol (b)* **238**, 68 (2003).
23. N. Yasuda, A. Kaneda, Z. Czapla, Effects of hydrostatic pressure on the paraelectric–ferroelectric phase transition in deuterated glycinium phosphite crystals. *J. Phys.: Condens Matter* **9**, L447 (1997).
24. Y. Shchur, A. Kityk. Piezoelectric properties of GPI crystals *Phys. Status Solidi B* **252**, 476 (2014).
25. A.S. Vdovych, I.R. Zachek, R.R. Levitskii, I.V. Stasyuk. Field-deformational effects in GPI ferroelectric materials. *Phase Transitions* **92**, 430 (2019).

Received 07.05.20

А.С. Вдович

ПОЗДОВЖНІЙ І ПОПЕРЕЧНИЙ
ЕЛЕКТРОКАЛОРИЧНІ ЕФЕКТИ
В СЕГНЕТОЕЛЕКТРИКУ ФОСФІТ ГЛІЦИНУ

Для дослідження електрокалоричного ефекту використано модифіковану модель протонного впорядкування сегнетоелектрика фосфіт гліцину, яка враховує п'єзоелектричний зв'язок протонної і ґраткової підсистем. Модель також враховує залежність ефективного дипольного моменту на водневому зв'язку від параметра впорядкування, а також розщеплення параметрів взаємодії між псевдоспінами при наявності зсувних деформацій. В наближенні двочастинкового кластера розраховано вплив поздовжнього та поперечного поля на компоненти вектора поляризації та тензора статичної діелектричної проникності кристала, а також на його теплові характеристики. Досліджено поздовжній і поперечний електрокалоричний ефект. Розрахована електрокалорична зміна температури виявилась досить малою, близько 1 K, проте вона може міняти знак під дією поперечного поля.

Ключові слова: фероелектрики, фазовий перехід, діелектрична проникність, ефект електричного поля, електрокалоричний ефект.